The functionally relevant site for paxilline inhibition of BK channels

Yu Zhou[a,1], Xiao-Ming Xia[a], and Christopher J. Lingle[a,1]

[a]Department of Anesthesiology, Washington University School of Medicine, St. Louis, MO 63110

Edited by Richard W. Aldrich, The University of Texas at Austin, Austin, TX, and approved December 4, 2019 (received for review July 22, 2019)

The tremorgenic fungal alkaloid paxilline (PAX) is a commonly used specific inhibitor of the large-conductance, voltage- and Ca^{2+}-dependent BK-type K^+ channel. PAX inhibits BK channels by selective interaction with closed states. BK inhibition by PAX is best characterized by the idea that PAX gains access to the channel through the central cavity of the BK channel, and that only a single PAX molecule can interact with the BK channel at a time. The notion that PAX reaches its binding site via the central cavity and involves only a single PAX molecule would be consistent with binding on the axis of the permeation pathway, similar to classical open channel block and inconsistent with the observation that PAX selectively inhibits closed channels. To explore the potential sites of interaction of PAX with the BK channel, we undertook a computational analysis of the interaction of PAX with the BK channel pore gate domain guided by recently available liganded (open) and metal-free (closed) *Aplysia* BK channel structures. The analysis unambiguously identified a preferred position of PAX occupancy that accounts for all previously described features of PAX inhibition, including state dependence, G311 sensitivity, stoichiometry, and central cavity accessibility. This PAX-binding pose in closed BK channels is supported by additional functional results.

K^+ channels | paxilline | BK channels | $Ca2^+$- and voltage-gated K^+ channels | mSlo1 channels

The identification and development of compounds that either inhibit or activate ion channels with high affinity and selectivity have been long-term, important quests not only for potential clinical applications, but also as tools for elucidating aspects of ion channel biophysics and physiology. For voltage-dependent ion channels, inhibitors are generally of 2 primary types: so-called open-channel blockers, in which a compound may simply occlude ion flux through open channels (1–3), and closed-channel blockers, in which drug binding essentially stabilizes channels in closed states (4–8). Although a physical picture of open-channel block is conceptually simple, closed-channel block may involve a number of mechanistically distinct categories, such as voltage-sensor stabilization (5–7) or drug binding at other positions that allosterically hinder the likelihood of channel opening (4, 8).

In general, our understanding of the structural and molecular basis of closed-channel block is rather minimal, and the nature of positions of drug binding that produce closed-channel block is not well defined. However, the hydrophobic nature of many closed-channels blockers has led to the idea that such components may reach their targets of action from a reservoir of inhibitory molecules within the plasma membrane (9, 10).

We recently reported that the tremorgenic fungal alkaloid paxilline (PAX) inhibits Ca^{2+}- and voltage-activated BK-type K^+ channels via an exclusively closed-channel block mechanism (8). PAX is one of a large number of related fungal alkaloids found in ryegrass for which the tremorgenic effects have been shown to arise from BK channel inhibition (11). The resulting "ryegrass staggers" syndrome results in appreciable economic loss of affected livestock (12). The functional evaluation of PAX closed-state inhibition, which was based on a well-established framework of BK channel gating (13–15), revealed that the primary determinant of the extent of inhibition by PAX was the steady-state open probability (P_O) during PAX application; inhibition was reduced or removed under conditions that favor high BK channel P_O and increased under conditions in which channels largely occupy closed states. Other functional features of the PAX inhibitory mechanism were identified as well. Block is best described by the idea that a single PAX molecule binds per channel, despite the 4-fold symmetry of the BK channel. Inhibition can be hindered by the simultaneous presence of the bulky open channel pore blocker, *N*-(4-[benzoyl]benzyl)-N,N,*N*-tributylammonium (bbTBA), and also by hyperosmotic sucrose at concentrations known to occupy a significant fraction of the central cavity volume (16). However, the presence of PAX in a BK channel does not prevent intracellularly applied 2-(trimethylammonium)ethyl methanethiosulfonate (MTSET) from modifying cysteines substituted for particular pore-lining residues (8). Furthermore, it has been shown that mutation of the so-called "hinge glycine" in BK S6 transmembrane segment to serine (G311S) or alanine (G311A) abolishes inhibition by PAX (17). Finally, the inner pore region of BK channel is likely to be exposed to the intracellular solution in both open and closed states, since BK channels lack a conventional cytosolic ion permeation gate (18–22). These observations suggest that PAX may access its blocking position via an aqueous pathway through the central cavity. Furthermore, the stoichiometry of one PAX molecule per channel suggests that any inhibitory site may involve the single central axis of the pore, a result generally expected for compounds acting as open-channel blockers.

Significance

Paxilline (PAX) is a specific BK channel inhibitor that has been widely used in various biophysical and physiological studies involving BK channels. It is also one of a few nonpeptidergic toxins with binding affinity comparable to that of peptidergic toxins. The current study identifies a binding pose of PAX in the closed BK channel that fits all known functional characteristics of PAX inhibition and is confirmed by additional functional tests. This result provides critical information to thoroughly understand the mechanism underlying BK channel inhibition by PAX, which will provide not only important insight into BK channel function, but also valuable guidance in the development of novel ion channel modulators.

Author contributions: Y.Z. and C.J.L. designed research; Y.Z. performed research; X.-M.X. contributed new reagents/analytic tools; Y.Z. analyzed data; and Y.Z. and C.J.L. wrote the paper.

The authors declare no competing interest.

This article is a PNAS Direct Submission.

Data deposition: The pdbqt files related to docking performed in this study are available at Open Science Framework, https://osf.io/cmy3e/.

[1]To whom correspondence may be addressed. Email: zhouy@wustl.edu or clingle@morpheus.wustl.edu.

This article contains supporting information online at https://www.pnas.org/lookup/suppl/doi:10.1073/pnas.1912623117/-/DCSupplemental.

First published December 26, 2019.

Here, to further probe the nature of the PAX blocking site, we used molecular docking to assess potential positions of PAX occupancy and to guide additional functional tests. To assess candidate PAX-binding sites, we generated 2 mammalian BK channel (mSlo1) homology models using the metal-free and liganded cryo-EM structures of the *Aplysia* BK (aSlo1) channels (22, 23), which for simplicity we refer to as "closed" and "open" models, respectively. Evaluation of docking identified a preferred PAX-binding site in a crevice between S6 and the pore helix (S6-PH crevice) that was occupied in the closed structural model but not in the open structural model. Furthermore, substitution of alanine or serine in the cognate G311 position abolished PAX occupancy in this crevice in the closed structure. Finally, when PAX occupies 1 of the 4 symmetric crevices near the entrance to the selectivity filter, a portion of PAX extends into the central cavity in a way that precludes accessibility of the other 3 crevices by additional PAX molecules. Thus, this site of PAX binding accounts for a unique set of functional characteristics of PAX inhibition, including closed-channel block, sensitivity to mutation of G311, stoichiometry of 1 site per channel, and accessibility from the central cavity. Based on this PAX-binding crevice, we confirmed in functional tests that the aSlo1 channel, which has a phenylalanine at the mSlo1 G311 position, is insensitive to PAX. In addition, guided by the PAX-binding pose in the closed mSlo1 pore, we identified 2 residues in the PAX-binding crevice, M285 in the PH and F307 in S6, that may stabilize PAX binding through a Met-aromatic interaction (24, 25) and a π-π stacking interaction (26), respectively. Mutations at these 2 sites reduced PAX sensitivity, confirming that the computationally identified site is the functionally relevant site of PAX inhibition.

Results

Molecular Docking Identifies a Single Site Likely to Explain All the Functional Features of BK Inhibition by PAX. As a heterocyclic compound, PAX is a largely rigid molecule (Fig. 1 and *SI Appendix*, Fig. S1). Being uncharged (pK_a = 13.56) with a single tertiary amine, it readily passes through membranes while also being water-soluble. Using 2 recently published aSlo1 channel cryo-EM structures as templates (22, 23), we generated homology models of mSlo1 for closed (Fig. 1*A*) and open (Fig. 1*B*) states, corresponding to sequences spanning the S0 to S6 transmembrane segments (*SI Appendix*, Fig. S2). Docking of PAX evaluated within the pore gate domain (PGD) of these 2 mSlo1 models (*SI Appendix*, Fig. S3) using AutoDock Vina (27) revealed distinct patterns of optimal binding poses.

In the closed mSlo1 pore, the most favored PAX binding pose is on the cytosolic side, with the indole ring of PAX inserted within the S6-PH crevice (Fig. 1 *A* and *C*). This binding pose is not only energetically more favored (*SI Appendix*, Fig. S4 and Table S1), but also fits all known functional characteristics of BK inhibition by PAX, as discussed below. Remarkably, this pose is not favored in the open mSlo1 pore; instead, the most favored PAX-binding site in the open mSlo1 pore is on the extracellular side, between the turret regions of 2 adjacent subunits (Fig. 1*B*). Interestingly, the extracellular occupancy of PAX in the open mSlo1 pore overlaps with that of charybdotoxin (CTX) (28) (*SI Appendix*, Fig. S5), perhaps in accordance with a previous study showing that PAX and other tremorgenic alkaloids can positively or negatively regulate binding of CTX to BK channels (29).

Functional data indicate that binding of only a single PAX molecule occurs in the PAX-inhibited BK channel (8), although the preferred PAX-binding site reflects 4 identical crevices. We therefore tested whether PAX occupancy of 1 S6-PH crevice might preclude occupancy of other identical crevices. When a single PAX molecule is manually predocked in the preferred binding site of the closed structure, the 2-propanol group at the C-15 of PAX extends at least 7 Å into the central cavity, essentially crossing the central axis of the pore (Fig. 1 *A*, *Inset*).

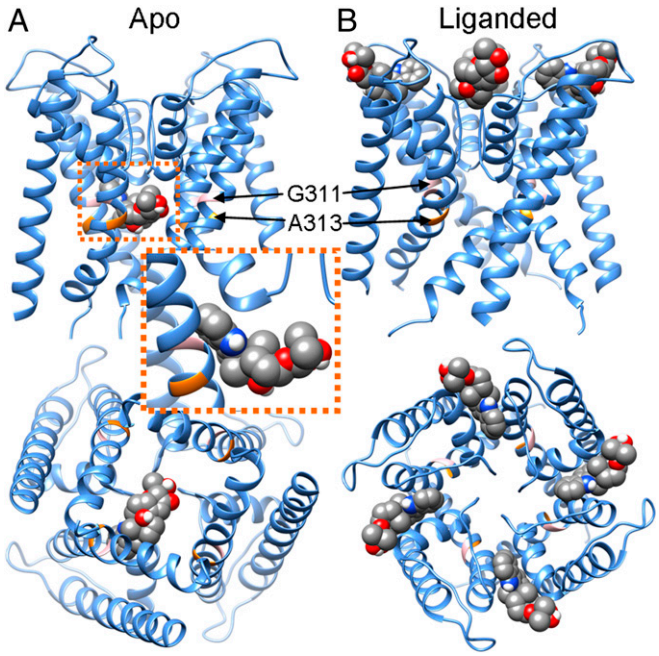

Fig. 1. The best docking poses of PAX in the pore region of the closed and open mSl1o homologous structures. (*A*) The best docking pose of PAX in the PGD of the closed mSlo1 structure. For clarity, only 1 of 4 identical binding poses is shown, as these poses partially overlap. PAX is rendered in spheres, with carbon, oxygen, nitrogen, and hydrogen shown in gray, red, blue, and white, respectively. (*Upper*) Side view. (*Lower*) View from the intracellular entrance of the BK channel. G311 and A313 are shown in pink and orange, respectively. (*Inset*) Close-up view of PAX in the closed BK pore. (*B*) The best docking pose of PAX in the open mSlo1 pore. (*Upper*) Side view. (*Lower*) View from the extracellular entrance of the BK channel.

PAX docking into the closed mSlo1 complex with 1 predocked PAX molecule shows that additional PAX molecules cannot access the remaining 3 binding crevices (*SI Appendix*, Fig. S6). Thus, once 1 PAX molecule is positioned in a crevice, it sterically hinders any other PAX molecule from accessing the other 3 identical sites.

This position of PAX occupancy in the closed mSlo1 structure also provides a simple explanation for 2 seemingly contradictory observations in previous work, that PAX competes with quaternary ammonium (QA) blockers in the BK inner pore region but does not prevent intracellularly applied MTSET from modifying cysteines substituting for a pore-lining residue (A313C) in the same region (8). As shown in *SI Appendix*, Fig. S7, PAX occupancy in the closed BK pore overlaps the position of pore occupancy by QA blockers, which is immediately below the K^+ channel selectivity filter (30). On the other hand, binding of a single PAX molecule does not preclude access of intracellularly applied MTSET to cysteine at position 313.

The most favored binding pose of PAX in the closed mSlo1 structure also accounts for 2 other features of PAX inhibition. First, closed channel inhibition occurs at 3 orders of magnitude lower PAX concentrations than open-state inhibition (8). Second, PAX inhibition is critically dependent on G311 in the mSlo1 S6; substitution of this glycine with either alanine or serine virtually abolishes BK sensitivity to PAX and other tremorgenic alkaloids (17). As shown in Figs. 1*A* and 2*A* and *SI Appendix*, Fig. S8, PAX fits tightly in the S6-PH crevice of the closed mSlo1 pore. The S6-PH crevice narrows during channel opening, with the distance between the α-carbons of G311 in S6 and M285 in the PH reduced from 7.1 Å in the closed structure to 5.5 Å in the open structure (Fig. 2 *A* and *B*). As a result, PAX is sterically

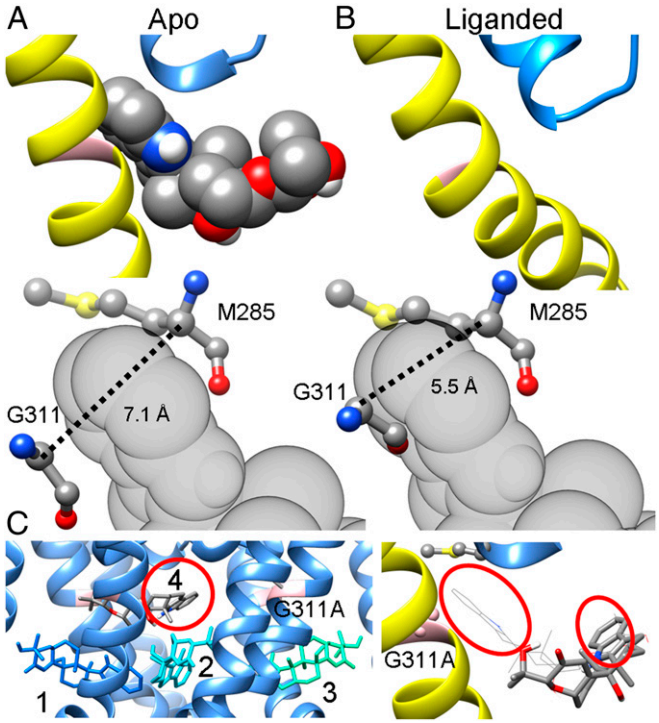

Fig. 2. Differences in the dimensions of the crevice between the PH and S6 account for the state dependence of PAX inhibition. (*A*, *Top*) The most favored binding pose of PAX in the metal-free BK pore, with S6 and the selectivity filter shown in yellow and blue, respectively. (*A*, *Bottom*) The relative position of PAX to G311 in S6 and M285 in the PH, 2 residues lining opposite faces of the binding crevice. The dotted line marks the distance between the α-carbons of G311 and M285. (*B*, *Top*) The open mSlo1 pore viewed from the same perspective as in *A*. (*B*, *Bottom*) The distance between the α-carbons of G311 and M285 decreases from 7.1 Å in the closed structure to 5.5 Å in the open structure. As a result, PAX cannot fit into the S6-PH crevice. (*C*, *Left*) The top 4 binding poses of PAX in the closed mSlo1G311A structure. G311A is shown in pink to indicate the location of the PAX-binding crevice. The numbers represent the rank order of binding poses, with 1 being the best binding pose. The relative energies of binding poses 1 to 4 calculated by AutoDock Vina are (in kcal/mol) −9.1, −9.1, −9.0, and −9.0, respectively. It should be noted that even though binding pose 4 is close to the binding crevice, the orientation of PAX is opposite to that observed in the WT structure, with the indole ring (red circle) pointing into the central cavity but not into the binding crevice as in the WT structure. (*C*, *Right*) Close-up view of the PAX binding pose 4 (rendered as sticks) in a closed mSlo1G311A pore, with the same perspective and coloring scheme as in *A* and *B*. The most favored binding pose of PAX in the WT BK pore (rendered as wires) is included for comparison. The indole rings of both binding poses are denoted by red circles.

precluded from entering the binding crevice of the open mSlo1 pore (Fig. 2*B*). The dimensional constraints of this crevice for PAX binding also explain the critical role of G311, since substitution of G311 with any other residue reduces the diameter of this binding crevice. In accordance with this, the most favored binding poses of PAX in a closed G311A pore are no longer found in this crevice (Fig. 2*C*).

Functional Tests of the Putative PAX-Binding Site. The PAX-occupied inhibitory crevice impressively accounts for a wide range of functional criteria, supporting the idea that this crevice defines the naturally occurring binding site. However, it would be desirable if the properties of this putative binding site led to other unique predictions.

aSlo1 is PAX-resistant. The aSlo1 channel sequence has a phenylalanine (F300) at the position homologous to mSlo1 G311 (23). If this binding crevice is universally the determinant of PAX sensitivity, then aSlo1 would be expected to be resistant to PAX. PAX docking in the pore region of the closed aSlo1 cryo-EM structure (22) shows that PAX preferentially resides in the gap between 2 adjacent subunits on the intracellular side (*SI Appendix*, Fig. S9 *A–C*). This binding position is intracellular to the 311 position, and PAX occupancy at this position is unlikely to occlude the ion permeation pathway or to stabilize closed states. In accordance with this, aSlo1 current is insensitive to 200 nM PAX (Fig. 3*A*), a concentration that completely blocks the mSlo1 BK current under similar conditions (Fig. 4*B*).

Using a chimeric surrogate, MC13, of the PAX-resistant Slo3 homolog of BK, it was previously shown that glycine substitution of S300, homologous to mSlo1 G311, can partially restore PAX sensitivity (17). In an attempt to restore PAX sensitivity in aSlo1, we replaced F300 with a glycine (aSlo1F300G). Interestingly, glycine substitution at this site negatively shifts the G-V of the resulting aSlo1 channels, even though the P_O of these channels is still very low, at 0 mV with 10 μM $[Ca^{2+}]_{in}$ (*SI Appendix*, Fig. S9 *F–H*). As shown in Fig. 3 *B* and *E*, 200 nM PAX has a very limited effect on aSlo1F300G. In MC13 and mSlo1, the residue before the hinge glycine site is also a glycine, while in aSlo1, the homologous residue is an isoleucine (I299). Glycine substitution at this position (I299G) in the background of aSlo1F300G partially restores PAX sensitivity to aSlo1 (aSlo1GG; Fig. 3 *D* and *F*), while aSlo1I299G itself is insensitive to PAX (Fig. 3 *C* and *E*). The fractional block by 200 nM PAX of aSlo1GG is comparable to that of MC13S300G. These results suggest that even though the hinge glycine is a prerequisite for BK inhibition by PAX, other structural elements that differ between aSlo1 and mSlo1 may also impact PAX sensitivity.

Mutations in the binding crevice reduce PAX sensitivity. Mutation of glycine hinders PAX inhibition by reducing the diameter of the S6-PH crevice, such that PAX is sterically prevented from entering the crevice. If in fact this crevice defines the native position of PAX inhibition, then mutation of other residues near G311 should also impact PAX sensitivity both experimentally

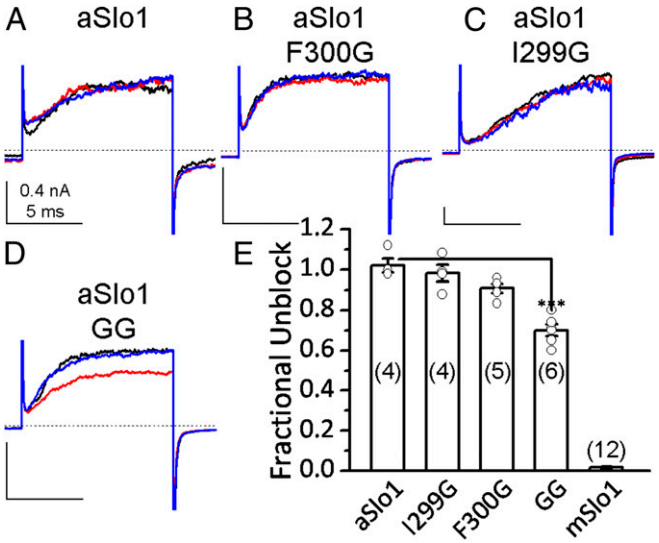

Fig. 3. The aSlo1 channel is insensitive to PAX. (*A–D*) Macroscopic currents of aSlo1 WT (*A*), F300G (*B*), I299G (*C*), and I299GF300G (*D*) evoked by +180-mV steps from a holding potential of 0 mV before application (black), in the presence (red), and washout (blue) of 200 nM PAX. Test pulse was applied every 5-s. $[Ca^{2+}]_{in}$ was 10 μM for all of the experiments shown in this figure. (*E*) Fractional unblock of aSlo1 and mSlo1 currents in the presence of 200 nM PAX at 0 mV with 10 μM $[Ca^{2+}]_{in}$. The number of experiments performed on each BK construct is in parentheses. The open circles represent the individual data points of aSlo1 inhibition by 200 nM PAX. ***$P = 0.0001$, 1-way ANOVA with the Bonferroni post hoc test.

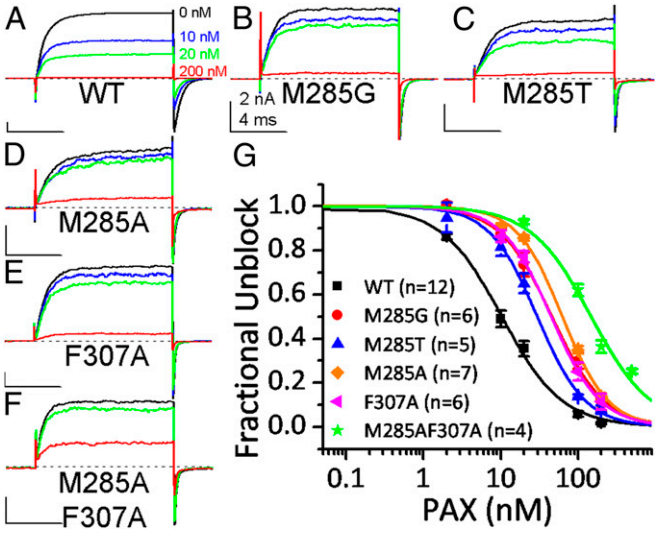

Fig. 4. Effect of binding crevice mutations on the PAX sensitivity of BK channels. WT or mutated BK channels were held at 0 mV with 10 μM $[Ca^{2+}]_{in}$ when exposed to various concentrations of PAX. BK current was evoked by a 10-ms step to 160 mV every 5 s to determine the fraction of unblocked channels. (*A–F*) The sample traces of WT (*A*), M285G (*B*), M285T (*C*), M285A (*D*), F307A (*E*), and M285AF307A (*F*) BK channels in 0 nM (black), 10 nM (blue), 20 nM (green), and 200 nM (red) PAX. The dotted line marks the 0-current level. (*G*) Dose–response curves of BK inhibition by PAX. Hill equation fit results (solid lines) are IC_{50} = 10.4 ± 0.6 nM, n = 1.1 ± 0.07 for WT (black symbol and line); IC_{50} = 46.3 ± 2.5 nM, n = 1.3 ± 0.07 for M285G (red symbol and line); IC_{50} = 29.9 ± 1.4 nM, n = 1.4 ± 0.07 for M285T (blue symbol and line); IC_{50} = 63.3 ± 3.3 nM, n = 1.5 ± 0.09 for M285A (orange symbol and line); IC_{50} = 45.4 ± 1.9 nM, n = 1.4 ± 0.05 for F307A (magenta symbol and line); and IC_{50} = 148.8 ± 9.1 nM, n = 1.1 ± 0.09 for M285AF307A (green symbol and line). The number of experiments contributing to each dose–response curve is in parentheses.

and perhaps computationally. Given the state dependence of PAX inhibition (8), it is important that a mutation at any such site not drastically change the gating of the resulting channels, as a mutation that favors open states will allosterically reduce apparent PAX sensitivity, while a mutation that strongly stabilizes closed states will make it difficult to obtain enough BK current to allow reliable measurement of any PAX effect.

Inspection of the favored PAX-binding pose in the closed mSlo1 structure identified 2 residues in the S6-PH crevice that may be positioned to mediate potential interactions with PAX (*SI Appendix*, Fig. S10*A*). One such residue is M285 in the mSlo1 PH. The center of the benzene ring of the PAX indole moiety lies 6.3 Å from the S_δ atom of M285 in the closed mSlo1 structure. Previous studies have shown that methionine is able to interact with an aromatic ring positioned 5 to 6 Å away, a common structural motif that stabilizes protein structure (24, 25). Thus, it seems possible that M285 forms a Met-aromatic interaction with PAX to stabilize PAX in the binding crevice. The second potential PAX-interacting residue is F307 in the mSlo1 S6. The distance between the centers of the benzene rings of PAX and F307 is 5.9 Å, which potentially allows the side chain of F307 to form an "edge-to-face" π-π stacking interaction with PAX (26).

To test whether these residues are involved in PAX interactions, we created 5 mSlo1 mutants: M285G, M285T, M285A, F307A, and M285AF307A. All these mutations moderately shifted BK gating toward positive potentials (*SI Appendix*, Fig. S10 *B–H*). Thus, any decrease in PAX sensitivity observed in these mutations should reflect a change in the binding affinity of PAX, but not from any allosteric effect arising from increased P_O of the resulting channels.

Fig. 4 *A–F* shows the macroscopic currents of WT channels and 5 binding crevice mutants before and after exposure to various concentrations of PAX. Following equilibration at 0 mV with 10 μM $[Ca^{2+}]_{in}$, 10 nM PAX blocks ∼50% of the current from WT channels, in agreement with the previously reported PAX IC_{50} of ∼10 nM under such conditions (8, 17, 29). Much less inhibition by 10 nM PAX is observed in M285G, M285T, M285A, and F307A under the same conditions. In addition, 200 nM PAX almost completely blocks WT BK current, while with M285G, M285T, M285A, and F307A, there remains an appreciable amount of residual current in the presence of 200 nM PAX. For M285AF307A double mutant, 200 nM PAX blocks ∼60% of the current. These observations indicate that mutations at positions M285 and F307 reduce PAX sensitivity.

The dose–response relationships of PAX inhibition on WT BK and 5 binding crevice mutations are shown in Fig. 4*G*. The IC_{50} of BK inhibition by PAX is increased from 10.8 nM in WT to 29.9 nM in M285T, 46.3 nM in M285G, 63.3 nM in M285A, 45.4 nM in F307A, and 148.8 nM in M285AF307A, corresponding to a change in PAX binding free energy (ΔG_{PAX}) of 0.6 kcal/mol by M285T, 0.9 kcal/mol by M285G, 1.0 kcal/mol by M285A, 0.9 kcal/mol by F307A, and 1.6 kcal/mol by M285AF307A. The ΔG_{PAX} of M285G or M285A is comparable to the strength of a Met-aromatic interaction, which provides an additional stabilization of 1 to 1.5 kcal/mol over a purely hydrophobic interaction (24). The smaller ΔG_{PAX} of M285T is in line with the fact that the side chain oxygen of threonine may also interact with aromatic ring, even though such interaction is weaker than the Met-aromatic interaction (24). The ΔG_{PAX} of F307A is compatible with a reduction in system energy of ∼1.0 kcal/mol by an "edge-to-face" π-π stacking interaction at a distance of 6 Å (26). The coupling free energy between M285 and F307 for PAX binding ($\Delta\Delta G_{PAX} = \Delta G_{PAX}^{M285AF307A} - \Delta G_{PAX}^{M285A} - \Delta G_{PAX}^{F307A}$) is only 0.3 kcal/mol, indicating that M285 and F307 interact independently with PAX in the binding crevice. These results are consistent with the idea that M285 and F307 are involved in PAX binding, thus supporting the view that the binding site identified by docking is the naturally occurring binding site of PAX in a closed BK channel.

We also attempted PAX docking in the closed mSlo1 model with the M285A or F307A mutation. A binding pose identical to the most favored binding pose in the WT mSlo1 model was identified in the S6-PH crevices of M285A, F307A, and M285AF307A mSlo1 models with the same binding energy as that of the WT mSlo1 model (*SI Appendix*, Fig. S11). The scoring function of AutoDock Vina is based on the X-Score function, which only includes terms for steric interactions, hydrogen bonding, hydrophobic interactions, and rotors (27). Thus, π-π stacking and Met-aromatic interactions are not fully considered, and the actual binding affinity of PAX in the S6-PH crevice of the WT mSlo1 is likely to be underestimated by AutoDock Vina. This may explain why the docking calculations in the mSlo1 models that include F307 and M285 binding crevice mutations fail to predict the functional impact of the mutations.

Docking of Other Tremorgenic Alkaloids in the Closed and Open BK Pores Identifies the Same Closed-State Binding Crevice. In addition to PAX, an extensive set of other fungal alkaloids, many of which are tremorgenic, have been shown to inhibit BK channels (29). In some cases, inhibition was shown to be G311-dependent (17). Therefore, we evaluated positions of occupancy of some of these alkaloids, including aflatrem, paspalicine, paspalinine, paspalitrem A, paspalitrem C, penitrem A, and verruculogen, using similar docking determinations. These tremorgenic alkaloids all exhibited preferred occupancy of the S6-PH crevice in the closed mSlo1 pore (*SI Appendix*, Fig. S12), but no occupancy of the same crevice in the open mSlo1 pore (*SI Appendix*, Fig. S13). Thus, alkaloids related to PAX exhibit the same state dependence of occupancy of the S6-PH crevice as PAX.

PAX Cannot Occupy the S6-PH Crevice of Other K^+ Channels. PAX is thought to be highly selective for BK channels at least in the sub-μM concentration range, but the S6-PH crevice is a common feature of all K^+ channels. Therefore, we evaluated PAX docking to 2 K^+ channels for which models of closed and open structures are available. The crystal structures of the KcsA channel have been solved in both closed (31) and wide open conformations (32), while a pair of Kv1.2 channel structural models in both resting/closed and activated/open states based on the Kv1.2 crystal structure (33) were constructed by Pathak et al. (34) using the RosettaMembrane method and molecular dynamics simulations. PAX docking in these 4 structures shows that none of the optimal PAX occupancy positions is in the S6-PH crevice of KcsA or Kv channels in either a closed or an open state (*SI Appendix*, Fig. S14). This arises because PAX sensitivity is critically dependent on the dimensions of the S6-PH crevice (Fig. 2 *A* and *B* and *SI Appendix*, Fig. S8). The S6-PH crevice of the KcsA and Kv channels (*SI Appendix*, Fig. S14 *C* and *F*, *Insets*) is considerably narrower than that of BK channel, especially the crevice in the closed BK channel (Fig. 2 *A* and *B*). Thus, the selectivity of PAX for the BK channel appears to arise from a wider S6-PH crevice in BK channels than is seen in other K^+ channels.

Discussion

The present docking analysis identifies a preferred position of PAX occupancy in the S6-PH crevice of the closed mSlo1 structural model. Before proceeding with the discussion, it is worth noting several major limitations of the docking procedure used here. First, the docking is done in the absence of water and ions. For binding poses in which PAX occupancies are in a narrow crevice within or between subunits, such as the primary binding pose in the S6-PH crevice, the influence of water and solutes may be less of a concern. However, for many other poses with large exposure of PAX to the aqueous milieu, such as those on the extracellular surface or in the spacious BK central cavity, we might expect that such positions and the estimated binding energies would be more impacted by water and solutes. Second, the approach evaluates a static protein and a static ligand. For PAX and some of its analogs, the heterocyclic nature of the compounds minimizes conformational flexibility, so the poses that are identified reflect a single static energy minimum rather than a family of closely related molecular positions. Finally, AutoDock Vina and other docking programs are limited in the types of energetic interactions they consider. For example, π-π interactions and Met-aromatic interactions are not fully considered in the scoring function of AutoDock Vina used here. As a result, the binding affinity of PAX in BK in the S6-PH crevice may be underestimated. Even though the current docking analysis by AutoDock Vina does a remarkable job in usefully identifying a plausible binding site of PAX in the closed mSlo1 model, a better understanding of the binding site and predictions based on it would require further improvement of the docking scoring function or other, more sophisticated analytical methods. This would also be critical for any future consideration of structure/function relationships with PAX derivatives.

That this S6-PH pose identified here is the true functionally relevant site responsible for BK inhibition by PAX is supported by the fact that this site explains a rather complex set of preexisting functional data. First, the preferred PAX occupancy in the S6-PH crevice occurs only with the closed mSlo1 structure and not with the open mSlo1 structure, consistent with the closed-state dependence of PAX inhibition (8). The state dependence of the occupancy arises from a narrowing of the S6-PH crevice in the open conformation. Second, replacing a conserved glycine (G311) at the entrance to the S6-PH crevice with other residues also prevents PAX from accessing its binding site by reducing the dimension of this crevice, consistent with the G311 sensitivity of PAX action (17). Third, only 1 of the 4 symmetric S6-PH crevices can be occupied at one time, because a portion of the PAX molecule when in its position of occupancy sterically prevents other PAX molecules from reaching the appropriate binding site. Finally, the route of access of the hydrophobic PAX molecule to its blocking site appears to be via an aqueous pathway through the central cavity of the BK channel. Overall, it seems highly improbable that a docking site would exhibit this set of features without it representing the correct, functionally relevant site of PAX action. Furthermore, the docking evaluation led to 2 predictions that were confirmed by functional results: (*i*) the aSlo1 channel, which lacks a glycine at the position homologous to mSlo1 G311, is insensitive to PAX, and (*ii*) M285 and F307 in the S6-PH crevice contribute to PAX binding.

The 2 most novel aspects of BK inhibition by PAX—the closed state dependence and G311 sensitivity—both arise from the narrow dimensions of the S6-PH crevice. The dimensional constraints provide a plausible explanation for the selectivity of PAX for BK channels. The width of this crevice, as defined by the distance of the α-carbons of 2 residues immediately across the crevice (G311 and M285), is reduced by >1.5 Å on opening (Fig. 2 *A* and *B*). Such a conformational change in a region close to the selectivity filter may be unique to the BK channel, which lacks a conventional cytosolic ion permeation gate (18–22), but which may rely on its selectivity filter to gate ion permeation. Although examples are limited, for K^+ channels with a conventional cytosolic ion permeation gate, such as KcsA and Kv channels, little or perhaps even an opposite conformational change is observed in this region on activation (*SI Appendix*, Fig. S14 *C* and *F*). The absence of an appreciable conformational change in the S6-PH crevice region during the gating of these channels, combined with the much narrower width of their S6-PH crevice, would appear to prevent PAX from accessing the S6-PH crevice of these channels in all functional states. Interestingly, the most favored position of occupancy of PAX in an open KcsA or Kv1.2 is found in the central cavity region of these channels (*SI Appendix*, Fig. S14 *B*, *C*, *E*, and *F*), raising the possibility that PAX might act as an open-channel blocker in these channels if the concentration of PAX is high enough. Given the abundance of distinct docking positions that PAX can occupy both in BK and in the KcsA and Kv1.2 models, we would caution that in cases where PAX is used experimentally at concentrations of 1 μM or higher, there remains the possibility that other nonspecific inhibitory effects of PAX may be revealed.

We also note that the present analysis may be relevant to earlier work that assessed the influence of PAX and other fungal alkaloids on CTX binding (28), in which it was proposed the PAX binding allosterically influences CTX binding at the extracellular mouth of the BK channel. Here the docking determinations reveal that the most favored position of occupancy of PAX and other tremorgenic alkaloids in the open mSlo1 pore is on the extracellular side (Fig. 1*B* and *SI Appendix*, Figs. S4 and S13 and Table S2), potentially overlapping with the CTX-binding site in K^+ channels (28). Therefore, we propose that the earlier observations of alkaloid effects on CTX binding may be better explained by alkaloid binding at secondary sites unrelated to the site of channel inhibition. Although an allosteric mechanism, as originally proposed (29), might help resolve the conflicting categories of effect, we prefer the view that, because all of the tremorgenic alkaloids have positions of occupancy on the extracellular surface of open BK channels, the specific positions they occupy may either impede or enhance CTX binding by direct interactions with CTX.

The relative absence of PAX docking poses on the extracellular side of the closed Slo1 model compared with that of the open model (e.g., Fig. 1*A* and *SI Appendix*, Fig. S4*A*) seem surprising, given the structural similarity of the extracellular face of the PGD in the 2 mSlo1 models (*SI Appendix*, Fig. S15*A*). Closer inspection of the most favored PAX occupancy position in the open mSlo1 model shows that the S1-S2 loop of the open mSlo1 model

(*SI Appendix*, Fig. S15*B*, green segment) is close to the PAX occupancy site and potentially contributes to PAX binding, while the same segment in the closed mSlo1 model (*SI Appendix*, Fig. S15*C*, yellow segment) is tilted away from the BK PGD and thus is less likely to interact with PAX docked in the BK PGD. Since this segment is not well resolved in the original aSlo1 structures (22, 23) and was generated by ab initio loop modeling in our mSlo1 models, we cannot draw conclusions regarding poses on the extracellular side between closed and open models. However, based on the docking to the open model, it seems likely that PAX can occupy positions on the extracellular side of the channel, albeit at binding affinities weaker than for the S6-PH crevice.

In summary, despite limitations of the docking methodology, the combination of a robust set of functional criteria allowed unambiguous identification of the likely functionally relevant site for PAX inhibition of BK channels. Most compellingly, the site revealed by docking allowed for the generation of new functional predictions that provide further confirmation that the critical PAX binding site has been identified.

Materials and Methods

Mutagenesis and Channel Expression. The pore-forming BK α-subunit used here were mouse mSlo1 α (GenBank accession no. NP_034740) (35) and *Aplysia* aSlo1 α (23). New mutations examined in this work included mSlo1 M285G, M285T, M285A, F307A, and M285AF307A and aSlo1 I299G, F300G, and I299GF300G. BK channels were expressed in stage IV *Xenopus* oocyte by RNA injection.

Homology Modeling and Docking. The homology models of the mSlo1 transmembrane domain (residues 1 to 331) were generated in Modeler 9.17 (36, 37) using the open and closed aSlo1 cryo-EM structures (22, 23) as templates. The sequence alignment for model building is shown in *SI Appendix*, Fig. S2. The segments missing in the cryo-EM aSlo1 structures were generated using the Loop modeling method (38) in Modeler. The structures of tremorgenic alkaloids were generated in Spartan 14 (Wavefunction Inc.) using the Hartree–Fock method with the 3-21G basis set. A single site mutation in the closed mSlo1 model was accomplished using the Swapaa function in UCSF Chimera (39). The structure of the PAX/closed mSlo1 pore complex was generated from the PDB files of closed mSlo1 and the most favored binding pose of PAX in closed mSlo1 using the combine function of UCSF Chimera. The structural images were also prepared using UCSF Chimera.

Docking of tremorgenic alkaloids into the mSlo1 PGD (residues 230 to 331) was performed in AutoDock Vina (27). A typical configuration file for docking can be found in *SI Appendix*, Table S3. No water, lipids, or ions are included in the docking system. The search space covers the entire BK PGD (*SI Appendix*, Fig. S3). AutoDock Vina estimates the binding energies of various docking poses through a combination of knowledge-based potentials and empirical scoring functions (27). Even though the binding energies predicted by AutoDock Vina correlate reasonably well with those determined experimentally, the SE between AutoDock Vina calculated energies and experimentally determined energies is ∼2.85 kcal/mol (27). Therefore, in this study, we simply ranked and compared binding poses returned by AutoDock Vina for a given docking run for a specific inhibitor and structural model, focusing on the highest-affinity poses.

Additional information on methods is provided in *SI Appendix*.

Data Availability. The pdbqt files of the 2 mSlo1 structural models and 8 fungal alkaloids and their typical binding poses have been uploaded to the Open Science Framework and are publicly available at https://osf.io/cmy3e/.

ACKNOWLEDGMENTS. We thank Dr. R. MacKinnon (The Rockefeller University) for generously providing the *Aplysia* BK construct. This work was supported by National Institute of General Medical Sciences Grant GM-118114 (to C.J.L.).

1. C. M. Armstrong, Inactivation of the potassium conductance and related phenomena caused by quaternary ammonium ion injection in squid axons. *J. Gen. Physiol.* **54**, 553–575 (1969).
2. C. M. Armstrong, B. Hille, The inner quaternary ammonium ion receptor in potassium channels of the node of Ranvier. *J. Gen. Physiol.* **59**, 388–400 (1972).
3. K. L. Choi, C. Mossman, J. Aubé, G. Yellen, The internal quaternary ammonium receptor site of Shaker potassium channels. *Neuron* **10**, 533–541 (1993).
4. Q. Luo *et al*., An allosteric ligand-binding site in the extracellular cap of K2P channels. *Nat. Commun.* **8**, 378 (2017).
5. K. J. Swartz, R. MacKinnon, Hanatoxin modifies the gating of a voltage-dependent K^+ channel through multiple binding sites. *Neuron* **18**, 665–673 (1997).
6. K. J. Swartz, R. MacKinnon, Mapping the receptor site for hanatoxin, a gating modifier of voltage-dependent K^+ channels. *Neuron* **18**, 675–682 (1997).
7. S. Y. Lee, R. MacKinnon, A membrane-access mechanism of ion channel inhibition by voltage sensor toxins from spider venom. *Nature* **430**, 232–235 (2004).
8. Y. Zhou, C. J. Lingle, Paxilline inhibits BK channels by an almost exclusively closed-channel block mechanism. *J. Gen. Physiol.* **144**, 415–440 (2014).
9. M. Arcisio-Miranda, Y. Muroi, S. Chowdhury, B. Chanda, Molecular mechanism of allosteric modification of voltage-dependent sodium channels by local anesthetics. *J. Gen. Physiol.* **136**, 541–554 (2010).
10. B. Hille, Local anesthetics: Hydrophilic and hydrophobic pathways for the drug-receptor reaction. *J. Gen. Physiol.* **69**, 497–515 (1977).
11. W. L. Imlach *et al*., The molecular mechanism of "ryegrass staggers," a neurological disorder of K^+ channels. *J. Pharmacol. Exp. Ther.* **327**, 657–664 (2008).
12. C. A. Morris, T. T. Wheeler, H. V. Henderson, N. R. Towers, S. H. Phua, Animal physiology and genetic aspects of ryegrass staggers in grazing sheep. *N. Z. Vet. J.* **65**, 171–175 (2017).
13. F. T. Horrigan, J. Cui, R. W. Aldrich, Allosteric voltage gating of potassium channels, I: Mslo ionic currents in the absence of Ca(2+). *J. Gen. Physiol.* **114**, 277–304 (1999).
14. F. T. Horrigan, R. W. Aldrich, Allosteric voltage gating of potassium channels, II: Mslo channel gating charge movement in the absence of Ca(2+). *J. Gen. Physiol.* **114**, 305–336 (1999).
15. F. T. Horrigan, R. W. Aldrich, Coupling between voltage sensor activation, Ca^{2+} binding and channel opening in large conductance (BK) potassium channels. *J. Gen. Physiol.* **120**, 267–305 (2002).
16. T. I. Brelidze, K. L. Magleby, Probing the geometry of the inner vestibule of BK channels with sugars. *J. Gen. Physiol.* **126**, 105–121 (2005).
17. Y. Zhou, Q. Y. Tang, X. M. Xia, C. J. Lingle, Glycine311, a determinant of paxilline block in BK channels: A novel bend in the BK S6 helix. *J. Gen. Physiol.* **135**, 481–494 (2010).
18. X. Chen, R. W. Aldrich, Charge substitution for a deep-pore residue reveals structural dynamics during BK channel gating. *J. Gen. Physiol.* **138**, 137–154 (2011).
19. C. M. Wilkens, R. W. Aldrich, State-independent block of BK channels by an intracellular quaternary ammonium. *J. Gen. Physiol.* **128**, 347–364 (2006).
20. Y. Zhou, X. M. Xia, C. J. Lingle, Cysteine scanning and modification reveal major differences between BK channels and Kv channels in the inner pore region. *Proc. Natl. Acad. Sci. U.S.A.* **108**, 12161–12166 (2011).
21. Y. Zhou, X. M. Xia, C. J. Lingle, Cadmium-cysteine coordination in the BK inner pore region and its structural and functional implications. *Proc. Natl. Acad. Sci. U.S.A.* **112**, 5237–5242 (2015).
22. R. K. Hite, X. Tao, R. MacKinnon, Structural basis for gating the high-conductance Ca^{2+}-activated K^+ channel. *Nature* **541**, 52–57 (2017).
23. X. Tao, R. K. Hite, R. MacKinnon, Cryo-EM structure of the open high-conductance Ca^{2+}-activated K^+ channel. *Nature* **541**, 46–51 (2017).
24. C. C. Valley *et al*., The methionine-aromatic motif plays a unique role in stabilizing protein structure. *J. Biol. Chem.* **287**, 34979–34991 (2012).
25. J. C. Gómez-Tamayo *et al*., Analysis of the interactions of sulfur-containing amino acids in membrane proteins. *Protein Sci.* **25**, 1517–1524 (2016).
26. G. B. McGaughey, M. Gagné, A. K. Rappé, pi-Stacking interactions. Alive and well in proteins. *J. Biol. Chem.* **273**, 15458–15463 (1998).
27. O. Trott, A. J. Olson, AutoDock Vina: Improving the speed and accuracy of docking with a new scoring function, efficient optimization, and multithreading. *J. Comput. Chem.* **31**, 455–461 (2010).
28. A. Banerjee, A. Lee, E. Campbell, R. Mackinnon, Structure of a pore-blocking toxin in complex with a eukaryotic voltage-dependent K(+) channel. *eLife* **2**, e00594 (2013).
29. H. G. Knaus *et al*., Tremorgenic indole alkaloids potently inhibit smooth muscle high-conductance calcium-activated potassium channels. *Biochemistry* **33**, 5819–5828 (1994).
30. M. J. Lenaeus, M. Vamvouka, P. J. Focia, A. Gross, Structural basis of TEA blockade in a model potassium channel. *Nat. Struct. Mol. Biol.* **12**, 454–459 (2005).
31. Y. Zhou, J. H. Morais-Cabral, A. Kaufman, R. MacKinnon, Chemistry of ion coordination and hydration revealed by a K^+ channel-Fab complex at 2.0 A resolution. *Nature* **414**, 43–48 (2001).
32. L. G. Cuello, V. Jogini, D. M. Cortes, E. Perozo, Structural mechanism of C-type inactivation in K(+) channels. *Nature* **466**, 203–208 (2010).
33. S. B. Long, E. B. Campbell, R. Mackinnon, Crystal structure of a mammalian voltage-dependent Shaker family K^+ channel. *Science* **309**, 897–903 (2005).
34. M. M. Pathak *et al*., Closing in on the resting state of the Shaker K(+) channel. *Neuron* **56**, 124–140 (2007).
35. X. M. Xia, X. Zeng, C. J. Lingle, Multiple regulatory sites in large-conductance calcium-activated potassium channels. *Nature* **418**, 880–884 (2002).
36. A. Sali, T. L. Blundell, Comparative protein modelling by satisfaction of spatial restraints. *J. Mol. Biol.* **234**, 779–815 (1993).
37. A. Sali, L. Potterton, F. Yuan, H. van Vlijmen, M. Karplus, Evaluation of comparative protein modeling by MODELLER. *Proteins* **23**, 318–326 (1995).
38. A. Fiser, R. K. Do, A. Sali, Modeling of loops in protein structures. *Protein Sci.* **9**, 1753–1773 (2000).
39. E. F. Pettersen *et al*., UCSF Chimera—A visualization system for exploratory research and analysis. *J. Comput. Chem.* **25**, 1605–1612 (2004).